Entropy **2015**, *17*, 7596-7607; doi:10.3390/e17117596

OPEN ACCESS

entropy

ISSN 1099-4300

www.mdpi.com/journal/entropy

Article

Single to Two Cluster State Transition of Primary Motor Cortex 4-posterior (MI-4p) Activities in Humans

Kazunori Nakada, Kiyotaka Suzuki and Tsutomu Nakada *

Center for Integrated Human Brain Science, Brain Research Institute, University of Niigata, Niigata 951-8585, Japan; E-Mails: Knakada@alumni.caltech.edu (K.N.); ksuzuki@bri.niigata-u.ac.jp (K.S.)

* Author to whom correspondence should be addressed; E-Mail: tnakada@bri.niigata-u.ac.jp; Tel.: +81-25-227-0677; Fax: +81-25-227-0821.

Academic Editor: Wassim M. Haddad

Received: 11 September 2015 / Accepted: 30 October 2015 / Published: 3 November 2015

Abstract: The human primary motor cortex has dual representation of the digits, namely, area 4 anterior (MI-4a) and area 4 posterior (MI-4p). We have previously demonstrated that activation of these two functional subunits can be identified independently by functional magnetic resonance imaging (fMRI) using independent component-cross correlation-sequential epoch (ICS) analysis. Subsequent studies in patients with hemiparesis due to subcortical lesions and monoparesis due to peripheral nerve injury demonstrated that MI-4p represents the initiation area of activation, whereas MI-4a is the secondarily activated motor cortex requiring a "long-loop" feedback input from secondary motor systems, likely the cerebellum. A dynamic model of hand motion based on the limit cycle oscillator predicts that the specific pattern of entrainment of neural firing may occur by applying appropriate periodic stimuli. Under normal conditions, such entrainment introduces a single phase-cluster. Under pathological conditions where entrainment stimuli have insufficient strength, the phase cluster splits into two clusters. Observable physiological phenomena of this shift from single cluster to two clusters are: doubling of firing rate of output neurons; or decay in group firing density of the system due to dampening of odd harmonics components. While the former is not testable in humans, the latter can be tested by appropriately designed fMRI experiments, the quantitative index of which is believed to reflect group behavior of neurons functionally localized, e.g., firing density in the dynamic theory. Accordingly, we performed dynamic analysis of MI-4p activation in normal volunteers and paretic patients. The results clearly indicated that MI-4p exhibits a transition from a single to a two phase-cluster state which coincided with loss of MI-4a activation. The study demonstrated

that motor dysfunction (hemiparesis) in patients with a subcortical infarct is not simply due to afferent fiber disruption. Maintaining proper afferent signals from MI-4p requires proper functionality of MI-4a and, hence, appropriate feedback signals from the secondary motor system.

Keywords: fMRI; independent component analysis; primary motor cortex; entrainment; synergetics

1. Introduction

It has been shown that digits and wrists within the primary motor cortex of non-human primates have double representation, namely, 4 rostral (MI-4r) and 4 caudal (MI-4c) [1,2]. Afferent inputs from digits and wrists to the primary motor cortex are similarly doubly represented. Substantial evidence has since been accumulated supporting that human MI also has two discrete areas of representation for the hands. The areas corresponding to primate MI-4r and MI-4c in the human are generally referred to as area 4 anterior (MI-4a) and area 4 posterior (MI-4p), respectively [3]. Utilizing an advanced functional magnetic resonance imaging (fMRI) technique based on independent component analysis, we have successfully demonstrated that these functional subunits of the primary motor cortex can be readily identified and quantitatively analyzed in humans *non-invasively* [4].

Subsequent studies in patients revealed that, while activation of MI-4p occurs in all subjects, regardless of severity of hand palsy, activation of MI-4a failed in patients with impaired "long-loop" feedback input from secondary motor systems, likely the cerebellum [5]. Given that MI-4p and MI-4a interact intimately with each other to produce proper hand motion, as suggested by non-human primate studies, lack of activation of MI-4a in hemiparetic patients may also indicate qualitative alteration of MI-4p activation (Figure 1). The successful stochastic modeling for self-organizing complex systems with robust applications was introduced by Haken and has been referred to as synergetics [6]. Subsequently, a dynamic model of hand motion based on the limit cycle oscillator has been extensively studied and the findings have been successfully implemented in accomplishing suppression of hand tremor in Parkinson's patients [7]. Application of this technique, deep brain stimulation (DBS), has now been extended to a variety of neurological disorders [8], underlining the importance of stochastic analysis of brain functionalities. One such modeling most successfully implemented for clinical applications is the phase resetting model presented by Tass [9] based on ensemble behavior of limit cycle oscillators. The Tass model provides not only a highly effective analytic tool for DBS, but also for various physiological data in humans including electroencephalography (EEG) and magnetoencephalography (MEG). The most intriguing aspect of the Tass model is its capability of observing synchronization of oscillators and alteration in patterns of their ensemble behavior associated with a given stimulation [9]. Since real time fMRI data are believed to reflect ensemble behavior of neurons synchronized for a given functionality [4,5,10], the Tass model can be utilized to test certain hypotheses in appropriately designed fMRI experiments.

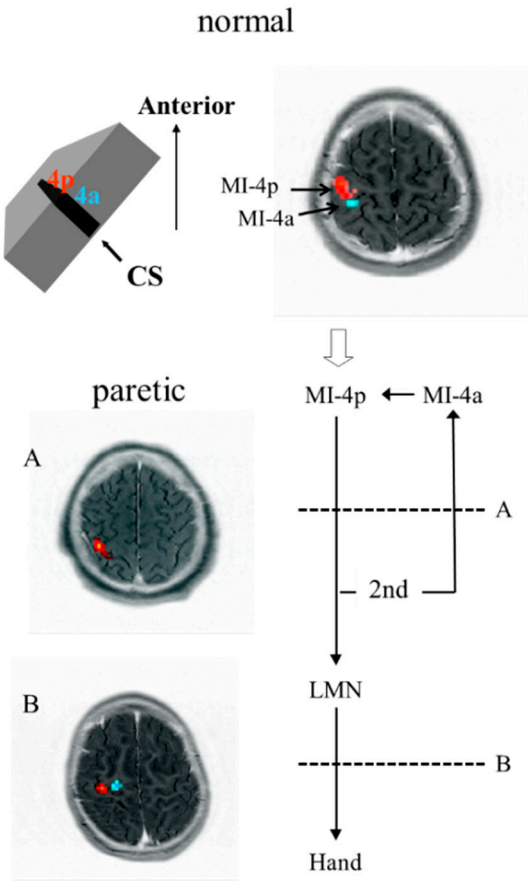

Figure 1. Schematic summary of the human primary somatosensory cortex organization. The primary motor cortex is located in the pre-central gyrus (Brodmann area 4). Human has dual representation of the digits, the areas of which are referred to as area 4 anterior (MI-4a) and area 4 posterior (MI-4p). While MI-4a is located closer to the surface of the brain, MI-4p is within the central sulcus (CS) [3]. The advanced technique in functional magnetic resonance imaging (fMRI) based on independent component analysis is capable to individually assess their functionality [4,5]. The independent components which show significant correlation ($r > 0.7$, $p < 0.001$) are extracted and displayed in the original two dimensional image matrix (fMRI images). MI-4p (red in fMRI) is an initiation area (open arrow in diagram), which is activated based on intention of the motion. MI-4a (green in fMRI) is the secondary area, the activation of which requires long loop feedback from the secondary motor system (2nd in diagram), the cerebellar system. Patients with hand paresis due subcortical lesion (dotted line A) cannot activate MI-4a, whereas patients with hand paresis due to a peripheral lesion (dotted line B) still show MI-4a activation. MI-4a, 4 anterior area of the primary motor cortex; MI-4p, 4 posterior area of the primary motor cortex; CS, central sulcus; LMN, lower motor neuron.

The model allows for analysis of specific entrainment firing pattern with appropriate periodic stimuli. Under normal conditions, such entrainment introduces a single phase-cluster. Under pathological condition where entrainment stimuli have insufficient strength, the phase cluster splits into two clusters [9]. Observable physiological phenomena of this single cluster to two clusters shift are: (1) doubling of firing rate in output neurons; or (2) decay in group firing density of the system due to

dampening of odd harmonics components (Figure 2). While the former is not testable in humans due to a lack of non-invasive methods capable of analyzing single neuron firing rates, the latter can be tested in humans by analyzing time series of appropriately designed fMRI experiments, the quantitative index of which is believed to reflect group behavior of neurons functionally localized, similar to those of the firing density defined in the entrainment theory.

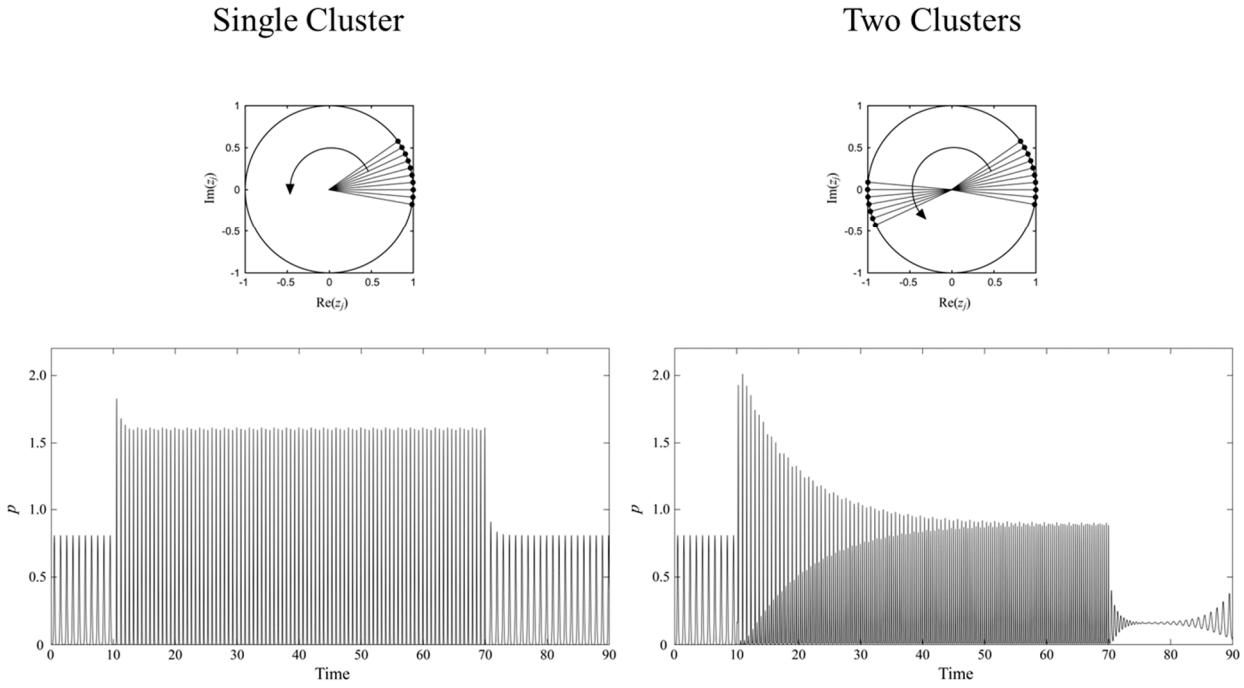

Figure 2. Simulated firing pattern. Cluster figures are redrawn based on the description of Tass [9]. The firing patterns were simulated utilizing Tass equation as described in Appendix. Observable physiological phenomena of the single cluster to two clusters shift are: (1) doubling of firing rate in output neurons; or (2) decay in group firing density of the system; due to damping of odd harmonic components. Although in animal experiments doubling in the firing rate can be directly examined by single cell recording, there is no non-invasive method applicable for humans. Nevertheless, with the appropriate fMRI paradigm, cluster changes can be examined as pattern changes in envelop of firing as schematically illustrated.

In this study, we tested the following hypotheses: (1) appropriately paced periodic voluntary motion of the corresponding hand can effectively introduce the conditions to which the entrainment model of dynamic theory of Tass can apply; (2) appropriately paced periodic voluntary motion of the corresponding hand in patients who failed to activate MI-4a can introduce the conditions where insufficient entrainment stimuli result in splitting of the single phase cluster into two clusters; and (3) the entrainment patterns can be assessed by fMRI as activation pattern reflecting the firing density of MI-4p.

2. Reproduction of the Tass Entrainment Model

The entrainment model of Tass is given as:

$$\frac{\partial n(\psi,t)}{\partial t} = -\frac{\partial}{\partial \psi}\left\{n(\psi,t)\int_0^{2\pi} d\psi' M(\psi-\psi') n(\psi',t)\right\} - \frac{\partial}{\partial \psi} n(\psi,t) S(\psi,t) - \Omega \frac{\partial}{\partial \psi} n(\psi,t) + \frac{Q}{2}\frac{\partial^2 n(\psi,t)}{\partial \psi^2}$$

where $n(\psi, t)$ represents: Average number density of (neuronal) oscillator phase ψ at time t, $M(\psi)$: phase-difference-dependent mutual interactions, $S(\psi, t)$: Stimulation, Ω: Spontaneous synchronization frequency (eigenfrequency), and Q: Noise amplitude. Furthermore, average number density, $n(\psi, t)$, meets the following boundary and normalization condition, respectively [9]:

$$n(0,t) = n(2\pi,t)$$

$$\int_0^{2\pi} n(\psi,t)\, d\psi = 1$$

Full discussion of the Tass equation is above the scope of this manuscript. Further description of its transformation into discrete functions is discussed in the Appendix. In short, we have successfully reproduced changes in the pattern of firing density, $p(t) = n(0, t)$, as described by Tass and shown in Figure 1. Numerical solutions of the differential equation were obtained on a 32-core shared memory Linux workstation (UV 2000 with 2.7 GHz Intel Xeon E5-4650 and 64 GB memory; SGI, Milpitas, CA, USA), using a parallelized scheme of the 4th order Runge–Kutta (RK4) method implemented on an in-house C program. The program code was compiled using Intel compiler version 13.0.1 and SGI message passing toolkit (MPT) library version 2.07. The results were plotted using MATLAB R2009B (The MathWorks, Natick, MA, USA) on a personal computer equipped with an Intel Core i7 processor. The simulation successfully reproduced the results shown by Tass (Figure 1).

3. Functional MRI

3.1. Subjects

Five normal volunteers and five subjects who had chronic (more than six months) hemiparesis due to a subcortical infarction participated in the study. Three subjects with chronic monoparesis (due to perinatal brachial plexus injury), in whom feedback from the secondary motor system was intact, were tested as pathological control. All "paretic" subjects had minor residual function of the corresponding paretic hand showing trace motion of the fingers as detectable by visual observation (Stage 3 of the Brunnstrom's classification [11]). All studies were performed according to the human research guidelines of the Internal Review Board of the University of Niigata.

Voluntary motion of the hand comprised perform smooth, self-paced grasp motions with one hand at a constant rate of one grasp per second. The performance of constant grasping was monitored by CCD camera placed in the magnet room. A total of nine thirty-second epochs were organized in boxcar configuration in RMRMRMRMR sequence where R and M indicates rest and motion, respectively. For prolonged studies, the study sequence was extended as follows: RRMMMMMMR.

3.2. Data Acquisition and Processing

Images were obtained using a General Electric Signa-prototype 3.0 T system equipped with an Advanced NMR echo-planar imaging (EPI) module. Gradient echo echo-planar axial images (GE-EPI) were obtained with the following parameter settings: FOV 40 cm × 20 cm; matrix 128 × 64; slice thickness 5 mm; TR 1 sec. Spatial resolution was approximately 3 mm × 3 mm × 5 mm. To obtain high field homogeneity, each slab was restricted to 30 mm. Each slab, which consisted of four consecutive 5-mm slices with inter-slice gap of 2.5 mm, was obtained in a single session.

Following application of spatial smoothing using a 5-mm full width at half maximum (FWHM) kernel, fMRI time series data consisting of 270 consecutive EPI images for each slice were subjected to independent component analysis implemented as described by McKeown *et al.* [12]. The process used an infomax neural network that employed stochastic gradient ascent to find a square unmixing matrix which maximized the joint entropy of a nonlinearly transformed ensemble of zero-mean input vectors. Logistic infomax could accurately decompose mixtures of component processes which had a symmetric or skewed distribution, even without the use of specifically tailored non-linearity [13–16].

In brief, joint entropy maximization was performed on the input data after they had been linearly transformed and then compressed by a nonlinear sigmoidal function: $y(t) = g\,[u(t)]$, where $u(t) = Wx(t) + W_0$. Before training, W was initialized to the identity matrix, I and W_0 to 0. W and W_0 were iteratively adjusted using small batches of randomly selected data vectors according to:

$$\Delta W = \varepsilon\left(\frac{\partial H(y)}{\partial W}\right)W^T W = \varepsilon\left(1 + \phi u(t)^T\right)W$$

$$\Delta W_0 = \varepsilon\,\phi(t)$$

where $H(y)$ was the joint entropy of y, ε the learning rate and the function $\varphi(t)$ had elements:

$$\phi_i(t) = \frac{\partial}{\partial u_i(t)}\ln\left(\frac{\partial y(t)}{\partial u_i(t)}\right)$$

The logistic nonlinearity gave a simple update rule:

$$\phi_i(t) \to 1 - 2y_i(t)$$
$$w_0(t) \to \varepsilon\left(1 - 2y_i(t)\right)$$

that biased the algorithm towards finding sparsely activated independent components with positive kurtosis [14]. Training was halted when the learning rate decreased below 0.000001.

Subsequently, 270 unmixed independent time series were subjected to cross correlation analysis using a delayed (6 seconds) boxcar model function reflecting one of the six sequential epoch patterns [4,5]. The independent components which showed significant correlation ($r > 0.7$, $p < 0.001$) were extracted and displayed in the original two dimensional image matrix (fMRI images). Anatomical

identification of activated areas was performed individually by mapping these onto each of the subject's own high resolution anatomical images obtained using identical coordinates. Reproducibility of the findings reported here was confirmed individually in each of the subjects.

3.3. Results

All subjects showed activation of MI-4p, while activation of MI-4a was not observed in patients who had a subcortical lesion, as shown in previous studies [4,5]. MI-4a was activated in normal and pathological (patients with monoparesis due to peripheral nerve lesion) controls. Representative time series of MI-4p activation are shown in Figure 3. The abscissa represents time in seconds, whereas the ordinate represents percent mean intensity changes. MI-4p activation in normal and pathological controls (peripheral) where MI-4a activation was observed showed the pattern indicating single cluster with appropriate entrainment stimuli regardless of functional condition, whereas MI-4p activation in patients who showed no MI-4a activation (subcortical) showed the pattern indicating its split into two clusters due to insufficient entrainment stimuli. Prolonged studies for normal control and subcortical patients, shown in Figure 4, clearly exhibited the predicted envelope pattern.

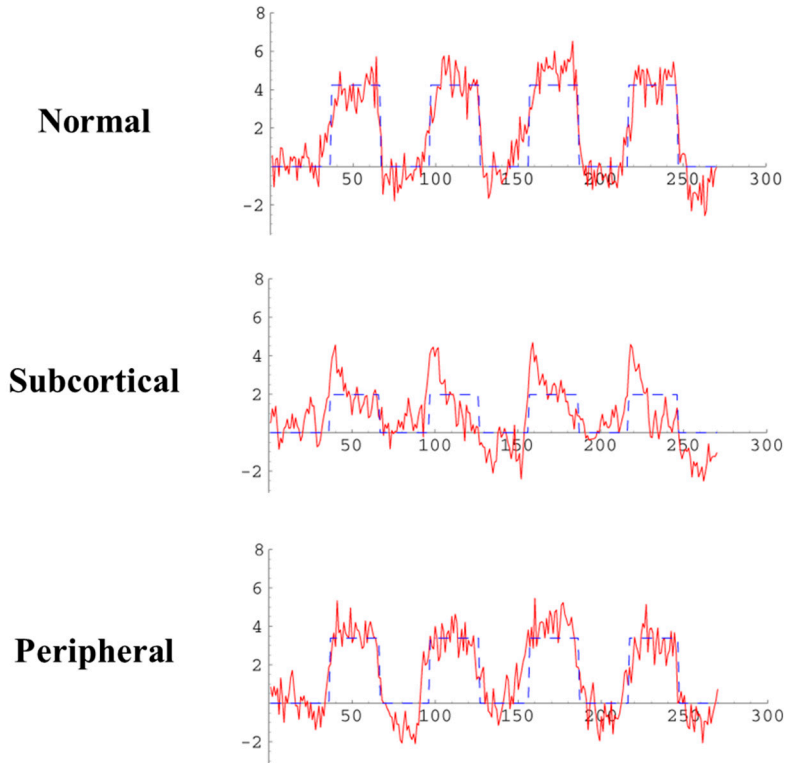

Figure 3. fMRI time series. Red graphs indicate representative time series of independent components obtained with RMRMRMR sequence where R and M indicate rest and motion, respectively. Blue lines represent the 6 second delayed boxcar model function applied for cross correlation analysis. The abscissa indicates time in seconds and the ordinate indicates percent mean intensity change. While normal subjects and patients with a peripheral lesion showed box car like activation pattern, patients with a subcortical lesion, who lack MI-4a activation, showed a clear decay with time.

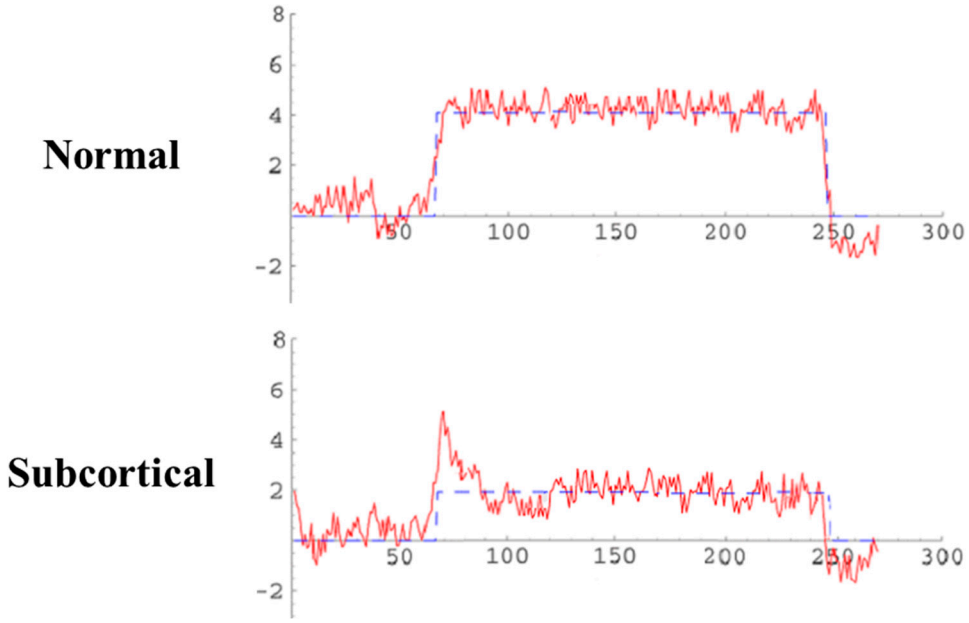

Figure 4. fMRI time series of prolonged motion study. In order to clearly identify an envelop pattern, prolonged motion studies with RRMMMMMMR sequence were performed. Patterns of activations of MI-4p for normal subjects and patients with a subcortical lesion clearly exhibited predicted patterns of single and two clusters shown in Figure 2.

4. Discussion

The discovery of the action potential and subsequent investigations led to the establishment of the field of mathematical modeling of brain activities based on the evaluation of single neuron activities as oscillator. It soon became apparent that synchronization of oscillatory neural activities represents a fundamental mechanism for integrating brain functionalities [17]. Pioneered by Winfree, practical medical applications have emerged from studies regarding the impact of external stimuli on a single oscillator [18]. The most successful example in clinical neurology remains to be the suppression of tremor in Parkinson patients by deep brain stimulation [7,8].

While ensemble of oscillatory neurons is key to various brain functionalities, it is fundamentally difficult to study neural activities directly in animals, let alone humans. Fortunately, group behavior of neurons responsible for a specific function can be directly observed in humans by means of functional imaging [10]. In this study, we investigated whether or not time series analysis of fMRI can be effectively utilized for assessing stochastic models of phase resetting presented by Tass [9]. The results clearly indicated that single cluster to two cluster splitting and resultant changes in entrainment patterns of target group of oscillators can be demonstrated by changes in firing patterns predicted by the model as a envelop of fMRI time series.

Identification of double representation of the digits within the primary motor cortex in humans, MI-4p and MI-4a, has introduced another window of motor system organization for voluntary motion [3–5]. This dual system for motor control is similar to another well-known motor control system of the humans, *i.e.*, pursuit eye movement. In order to maintain proper pursuit, one has to have a system capable of accurately cancelling head motion. The primary system is the vestibular-ocular reflex (VOR) which is fine-tuned by secondary modifiable cerebellar learning units [19]. MI-4p is the primary system

for voluntary hand motion. Nevertheless, in order to perform fine motions by digits, activities of MI-4p is modified by MI-4a which is fine tuned by feedback signals from the cerebellum. It is highly conceivable to conclude that systems performing fine movements, such as pursuit eye movements or voluntary hand motion, require dual motor control systems.

Significant modification of MI-4p activities resulting from lack of proper entrainment stimuli from MI4a has strong clinical implications, providing hitherto unrecognized factors for the treatment of disturbed motor systems in humans. Motor dysfunction (hemiparesis) in patients with a subcortical infarct is generally believed to be due to disruption of efferent fibers within corticospinal (pyramidal) tract. The current study indicated that this is not the case. Maintaining proper afferent signals from MI-4p actually requires proper functionality of MI-4a and, hence, proper feedback signals from the secondary motor system, *i.e.*, the cerebellum. While applications of machine-brain interface and biomechanics for various clinical conditions are becoming common in neuroscientific investigations, the current study emphasizes the necessity of further understanding of underlying anatomical mechanisms of fine motor controls.

Acknowledgments

The work was supported by grants from the Ministry of Education, Culture, Sports, Science, and Technology (Japan) and University of Niigata.

Author Contributions

Kazunori Nakada designed the concept, did data acquisition, data analysis and wrote the manuscript. Kiyotaka Suzuki did data acquisition and data analysis. Tsutomu Nakada designed the concept and wrote the manuscript. All authors have read and approved the final manuscript.

Conflicts of Interest

The authors declare no conflict of interest.

Appendix

Discrete version of the Tass equation utilized is given as follows:

$$\begin{aligned}\frac{\partial \hat{n}(k,t)}{\partial t} = & -ik\sum_{\pm m=1}^{4}\hat{M}(m)\hat{n}(k-m,t)\hat{n}(m,t) \\ & -ik\sum_{\pm m=1}^{4}\hat{n}(k-m,t)\hat{S}(m) \\ & -ik\Omega\hat{n}(k,t) \\ & -\frac{Q}{2}k^2\hat{n}(k,t)\end{aligned} \tag{A1}$$

where

$$\sum_{\pm m=1}^{4} \lambda_m \equiv \lambda_1 + \lambda_2 + \lambda_3 + \lambda_4 + \lambda_{-1} + \lambda_{-2} + \lambda_{-3} + \lambda_{-4} \tag{A2}$$

$\hat{n}$ is complex. However, based on the boundary and normalizing conditions shown in the text, n can be treated as a positive real number and, therefore:

$$\hat{n}(0,t) = \frac{1}{2\pi}, \text{ for all times } t \tag{A3}$$

$$\hat{n}(-k,t) = \hat{n}^*(k,t), \text{ for all wave numbers } k \text{ and for all times } t \tag{A4}$$

For discrete form for M and S, the following equations were adopted:

$$M(\psi_j - \psi_k) = -\sum_{m=1}^{4} \left\{ K_m \sin\left[m(\psi_j - \psi_k) \right] + C_m \cos\left[m(\psi_j - \psi_k) \right] \right\} \tag{A5}$$

$$S(\psi_j, t) = \sum_{m=1}^{4} I_m \cos\left[m(\psi_j - \omega t) + \gamma_m \right] \tag{A6}$$

Accordingly:

$$n(\psi, t) = \sum_{k \in \mathbf{Z}} \hat{n}(k, t) e^{ik\psi} \tag{A7}$$

$$M(\psi - \psi') = \sum_{k \in \mathbf{Z}} \hat{M}(k) e^{ik(\psi - \psi')} \tag{A8}$$

$$S(\psi) = \sum_{k \in \mathbf{Z}} \hat{S}(k) e^{ik\psi} \tag{A9}$$

Due to its periodicity, $\hat{M}$ can be given:

$$\hat{M}(k) = \begin{cases} \pi(-C_k + iK_k): & k = 1, 2, 3, 4 \\ -\pi(C_{-k} + iK_{-k}): & k = -1, -2, -3, -4 \\ 0: & otherwise \end{cases} \tag{A10}$$

Without stimuli, time progression of n was obtained by translating $\hat{n}$ into n following integrating the Tass Equation (A1) with $\hat{S}$ = 0. With smooth periodic stimulation shown in Equation (A6), time progression of n was obtained by utilizing the fact that for θ defined as:

$$\theta_j(t) = \psi_j(t) - \omega t \tag{A11}$$

The following equations for $\hat{n}$, $\tilde{S}, \tilde{\Omega}$ can satisfy the Tass Equation (A1):

$$n(\theta, t) = \sum_{k \in \mathbf{Z}} \hat{n}(k, t) e^{ik\theta} \tag{A12}$$

$$\tilde{S}(\theta_j) = \sum_{m} I_m \cos(m\theta_j + \gamma_m) \tag{A13}$$

$$\tilde{\Omega} = \Omega - \omega \tag{A14}$$

Based on periodicity, Fourier representation of the stimulation, $\hat{S}$ is given as:

$$\hat{S}(k)=\begin{cases} I_k \exp[i\gamma_k]/2: & k=1,2,3,4 \\ I_{-k} \exp[-i\gamma_{-k}]/2: & k=-1,-2,-3,-4 \\ 0: & otherwise \end{cases} \quad \text{(A15)}$$

Subsequently, $n(\psi, t)$ can be determined by utilizing Equations (A11)–(A14).

For actual calculation, the following parameters have been utilized.

Spontaneous synchronization frequency (eigenfrequency):

$\Omega = 2\pi$

Noise level:

Q = 0.4

Interaction (coupling) parameters:

$K_1 = 1$, $K_2 = K_3 = K_4 = 0$

$C_1 = C_2 = C_3 = C_4 = 0$

Stimulation parameters:

$\omega = 3\pi$

$I_1 = 4$, $I_2 = I_3 = I_4 = 0$ for single cluster

$I_2 = 4$, $I_1 = I_3 = I_4 = 0$ for two clusters

$\gamma_1 = \gamma_2 = \gamma_3 = \gamma_4 = 0$

References

1. Strick, P.L.; Preston, B. Two representations of the hand in area 4 of a primate. I. Motor output organization. *J. Neurophysiol*. **1982**, *48*, 139–149.
2. Strick, P.L.; Preston, B. Two representations of the hand in area 4 of a primate. II. Somatosensory input organization. *J. Neurophysiol.* **1982**, *48*, 150–159.
3. Geyer, S.; Ledberg, A.; Schleicher, A.; Kinomura, S.; Schormann, T.; Bürgel, U.; Klingberg, T.; Larsson, J.; Zilles, K.; Roland, P.E. Two different areas within the primary motor cortex of man. *Nature* **1996**, *382*, 805–807.
4. Nakada, T.; Fujii, Y.; Suzuki, K.; Kwee, I.L. High-field (3.0T) functional MRI sequential epoch analysis: An example for motion control analysis. *Neurosci. Res.* **1998**, *32*, 355–362.
5. Nakada, T.; Suzuki, K.; Fujii, Y.; Matsuzawa, H.; Kwee, I.L. Independent component-cross correlation-sequential epoch (ICS) analysis of high-field fMRI time series: direct visualization of dual representation of the primary motor cortex in human. *Neurosci. Res.* **2000**, *37*, 237–244.
6. Haken, H. *Principles of Brain Functioning*; Springer: Berlin/Heidelberg, Germany, 1996.
7. Benabid, A.L.; Chabardes, S.; Mitrofanis, J.; Pollak, P. Deep brain stimulation of the subthalamic nucleus for the treatment of Parkinson's disease. *Lancet Neurol.* **2009**, *8*, 67–81.
8. Perlmutter, J.S.; Mink, J.W. Deep brain stimulation. *Ann. Rev. Neurosci.* **2006***, 29*, 229–257.
9. Tass, P.A. *Phase Resetting in Medicine and Biology*; Springer: Berlin/Heidelberg, Germany, 1999.
10. Nakada, T. Myths and truths in functional MRI: A basic guide for practitioners. *Magn. Reson. Med. Sci.* **2002**, 1, 89–107.
11. Brunnstrom, S. Motor testing procedures in hemiplegia: Based on sequential recovery stages. *Phys. Ther.* **1966**, *46*, 357–375.

12. McKeown, M.J.; Makeig, S.; Brown, G.G.; Jung, T.-P.; Kindermann, S.S.; Kindermann, R.S.; Bell, A.J.; Sejnowski, T.J. Analysis of fMRI data by blind separation into independent spatial components. *Hum. Brain Map.* **1995**, *6*, 160–188.
13. Comon, P. Independent component analysis: A new concept? *Signal Process.* **1994**, *36*, 287–314.
14. Bell, A.J.; Sejnowski, T.J. An information-maximization approach to blind separation and blind deconvolution. *Neural Comput.* **1995**, *7*, 1129–1159.
15. Makeig, S.; Jung, T.P.; Ghahremani, D.; Bell, B.J.; Sejnowski, T.J. Blind separation of auditory event-related brain responses into independent components. *Proc. Natl. Acad. Sci. USA* **1997**, *94*, 10979–10984.
16. Amari, S. National gradient works efficiently in learning. *Neural Comput.* **1998**, *10*, 251–276.
17. Singer, W.; Gray, C.M. Visual feature integration and the temporal correlation hypothesis. *Annu. Rev. Neurosci.* **1995**, *18*, 555–586.
18. Winfree, A.T. *The Geometry of Biological Time*; Springer: Berlin/Heidelberg, Germany, 1980.
19. Nakada, T.; Kwee, I.L. Oculopalatal myoclonus. *Brain* **1986**, *109*, 431–441.